

Supporting Information

***In-situ* QXAFS study on CO and H₂ adsorption on Pt in solid [PtAu₈(PPh₃)₈]-H[PMo₁₂O₄₀]**

Tomoki Matsuyama,^a Taishi Suzuki,^a Yuto Oba,^a Soichi Kikkawa,^a Sayaka Uchida,^b Junya Ohyama,^c Kotaro Higashi,^d Takuma Kaneko,^d Kazuo Kato,^d Kiyofumi Nitta,^d Tomoya Uruga,^d Keisuke Hatada,^e Kazuki Yoshikawa,^e Amelie Heilmaier,^{e,f} Kosuke Suzuki,^g Kentaro Yonesato,^g Kazuya Yamaguchi,^g Naoki Nakatani,^a Hideyuki Kawasoko,^{a,h} and Seiji Yamazoe^{*a}

^a Department of Chemistry, Graduate School of Science, Tokyo Metropolitan University, 1-1 Minamiosawa, Hachioji-shi, Tokyo 192-0397, Japan

^b Department of Basic Science, School of Arts and Sciences, The University of Tokyo, 3-8-1 Komaba, Meguro-ku, Tokyo 153-8902, Japan

^c Faculty of Advanced Science and Technology, Kumamoto University, 2-39-1 Kurokami, Chuo-ku, Kumamoto-shi, Kumamoto 860-8555, Japan

^d Center for Synchrotron Radiation Research, Japan Synchrotron Radiation Research Institute (JASRI), 1-1-1, Kouto, Sayo-cho, Sayo-gun, Hyogo 679-5198, Japan

^e Department of Physics, University of Toyama, 3190 Gofuku, Toyama 930-8555, Japan

^f Department of Chemistry, Ludwig-Maximilians-Universität (LMU), Butenandtstr. 5-13, 81377 Munich, Germany

^g Department of Applied Chemistry, School of Engineering, The University of Tokyo, 7-3-1 Hongo, Bunkyo-ku, Tokyo 113-8656, Japan

^h Precursory Research for Embryonic Science and Technology (PRESTO), Japan Science and Technology Agency (JST), 7, Gobancho, Chiyoda-ku, Tokyo 102-0076, Japan

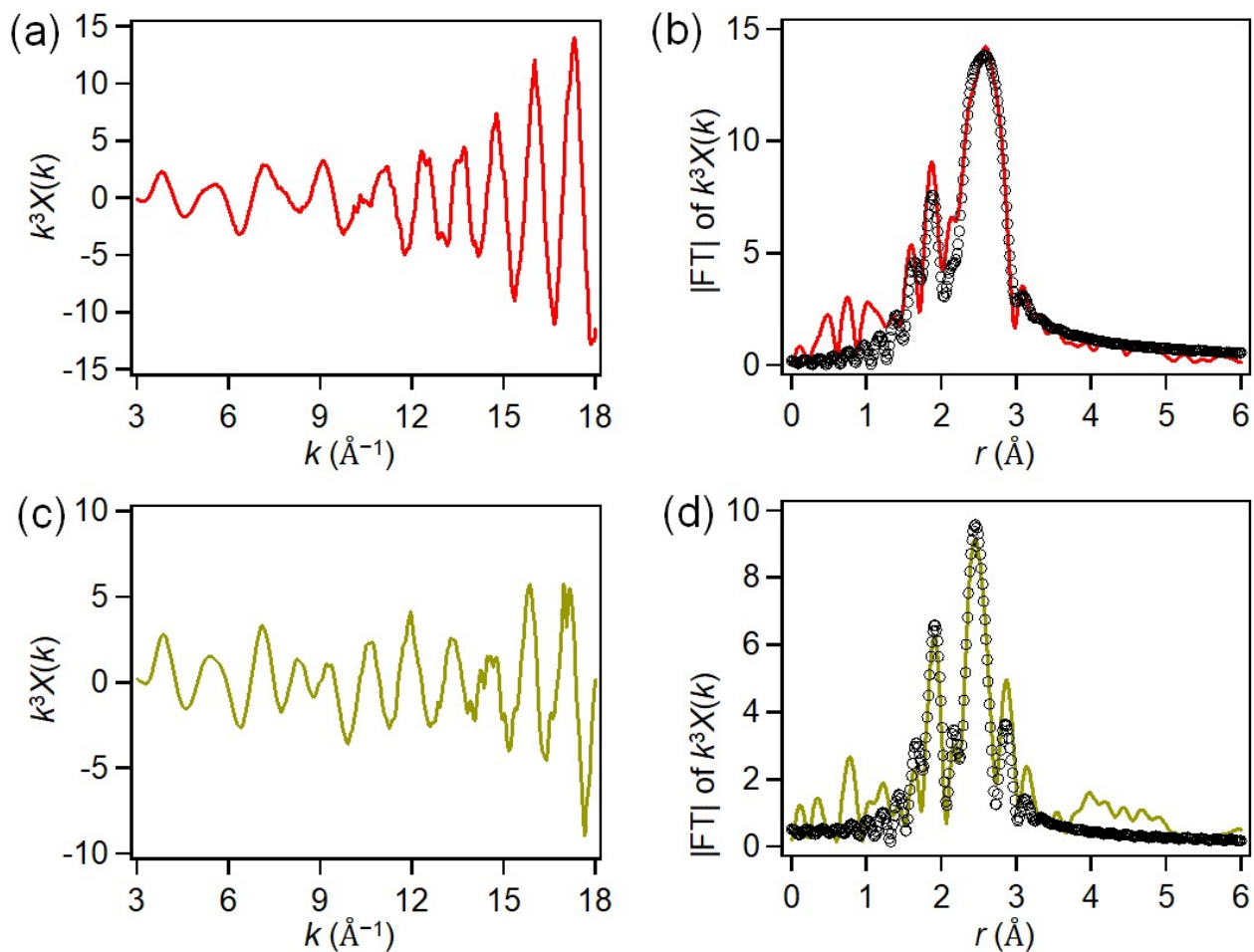


Fig. S1. Au L_3 -edge (a) EXAFS oscillation and (b) FT-EXAFS spectra of **PtAu8-PMo12**, and (c) EXAFS oscillation and (d) FT-EXAFS spectra of **Au9-PMo12** measured at 10 K. The circles in (b) and (d) represent the fitting curves, whose parameters and results are listed in Table S1.

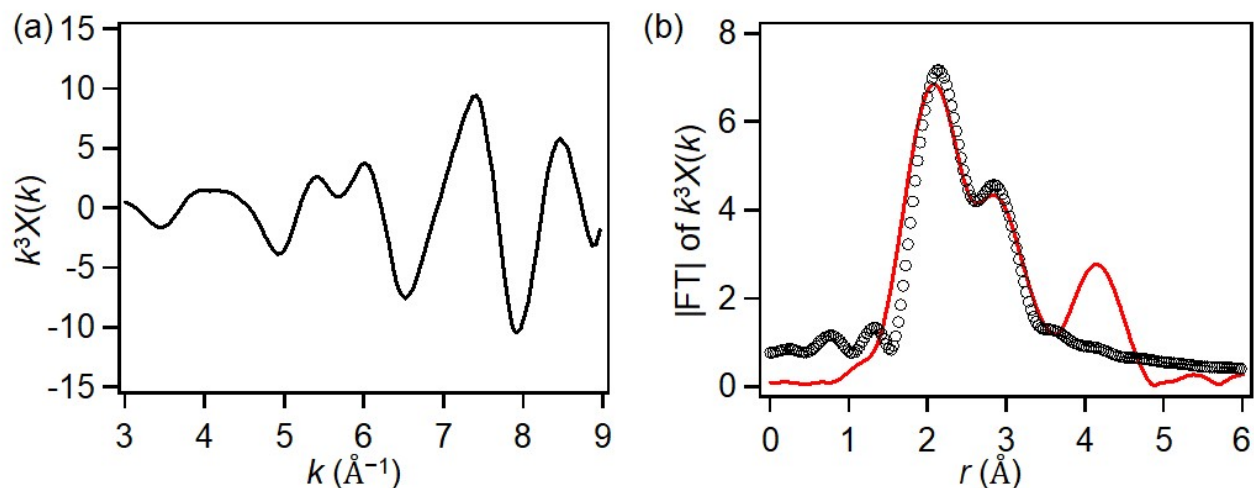


Fig. S2. Pt L_3 -edge (a) EXAFS oscillations and (b) FT-EXAFS spectra of **PtAu8-PMo12** measured at 10 K. The circles in (b) represent the fitting curves, whose parameters and results are listed in Table S2.

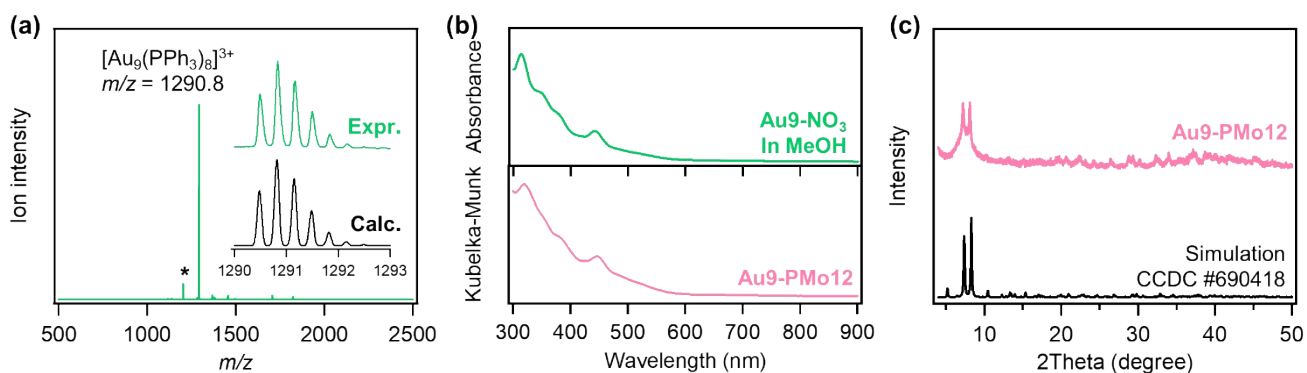


Fig. S3. Characterizations of **Au9-NO3** and **Au9-PMo12**. (a) Positive-ion mode ESI-MS of acetonitrile solution of **Au9-NO3**. Asterisk peak is the ligand-dissociated product in the analysis: $[\text{Au}_9(\text{PPh}_3)_7]^{3+}$. (b) UV-vis spectrum of methanolic solution of **Au9-NO3** and DR-UV-Vis spectrum of **Au9-PMo12**. (c) Powder-XRD pattern of **Au9-PMo12**.

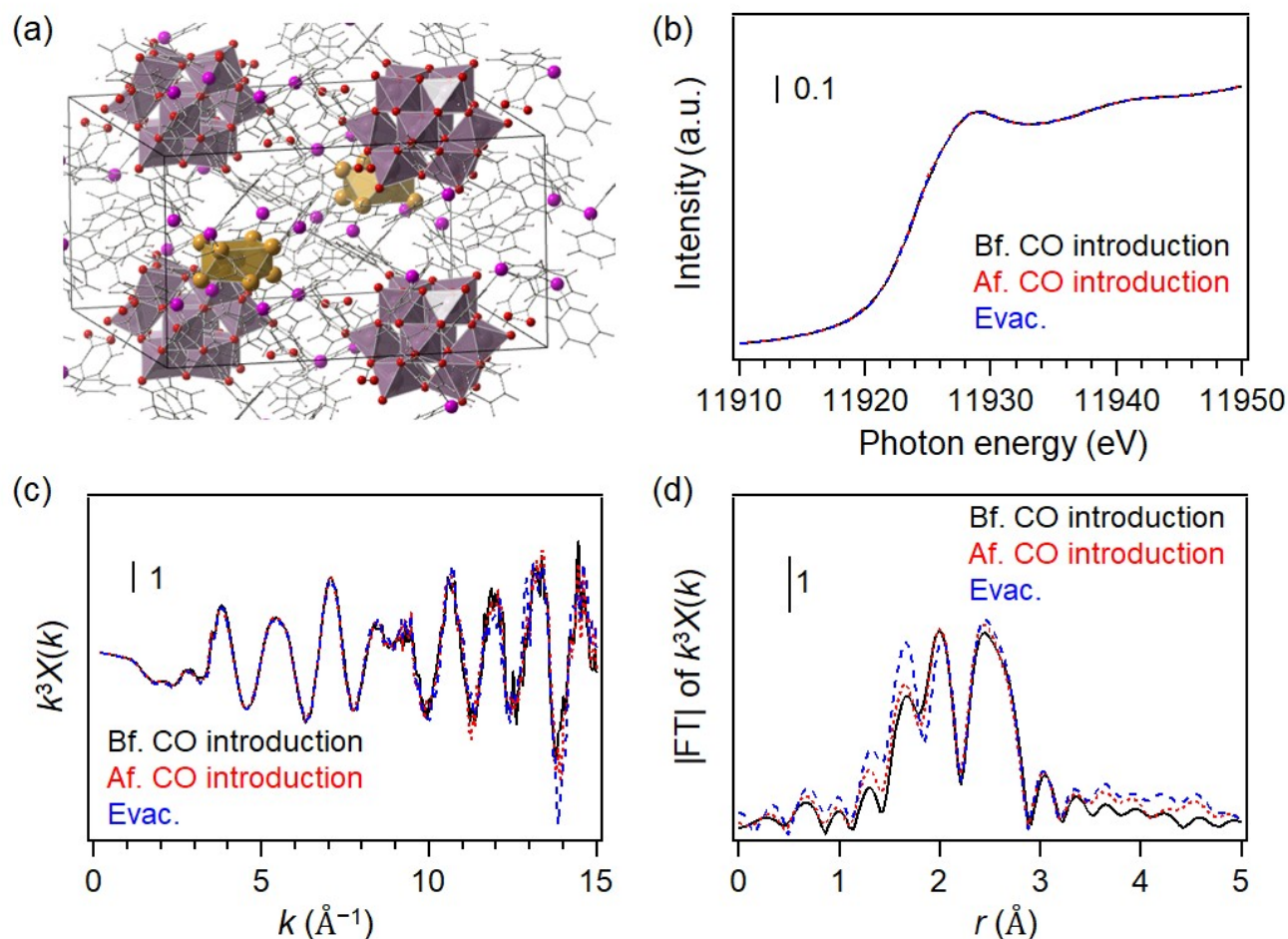


Fig. S4. (a) Crystal structure of **Au9-PMo12**.¹ Au L_3 -edge (b) XANES, (c) EXAFS oscillations, and (d) FT-EXAFS spectra of **Au9-PMo12** before CO introduction, after CO introduction, and then after evacuation.

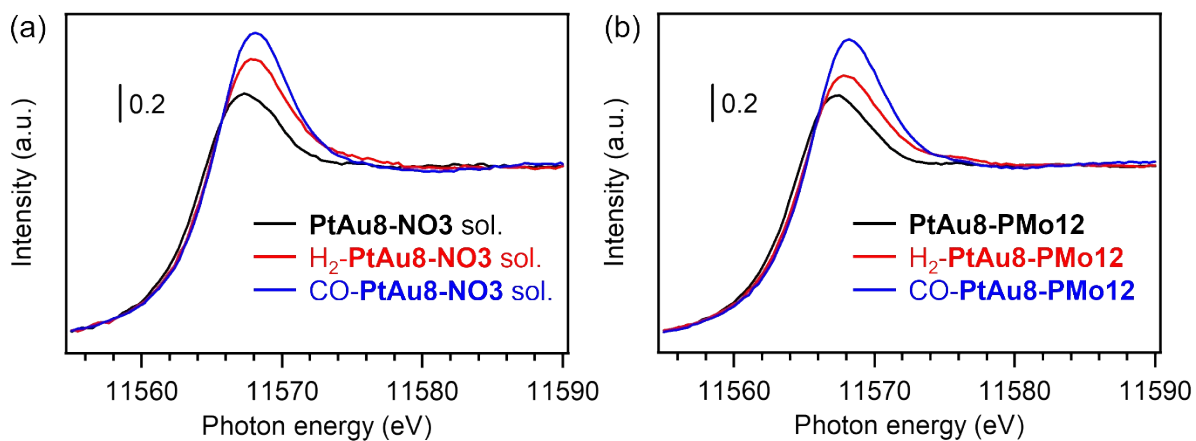


Fig. S5. Pt L₃-edge *in-situ* XANES spectra of (a) **PtAu8-NO3** in acetonitrile and (b) **PtAu8-PMo12** in the solid state. The XAFS data were measured in BL01B1 at SPring-8 facility with using Si(111) mirror to monochromize the incident X-ray.

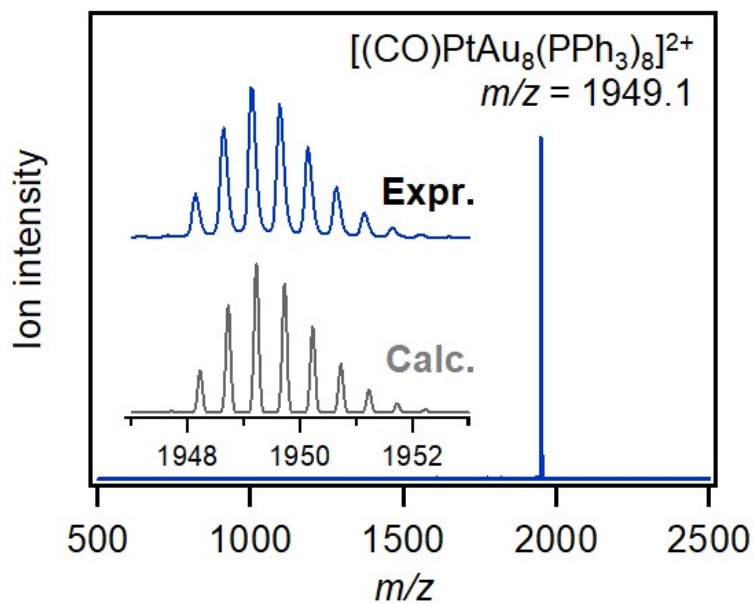


Fig. S6. Positive-ion mode ESI-MS of **CO-PtAu8-PMo12** dissolved in acetonitrile.

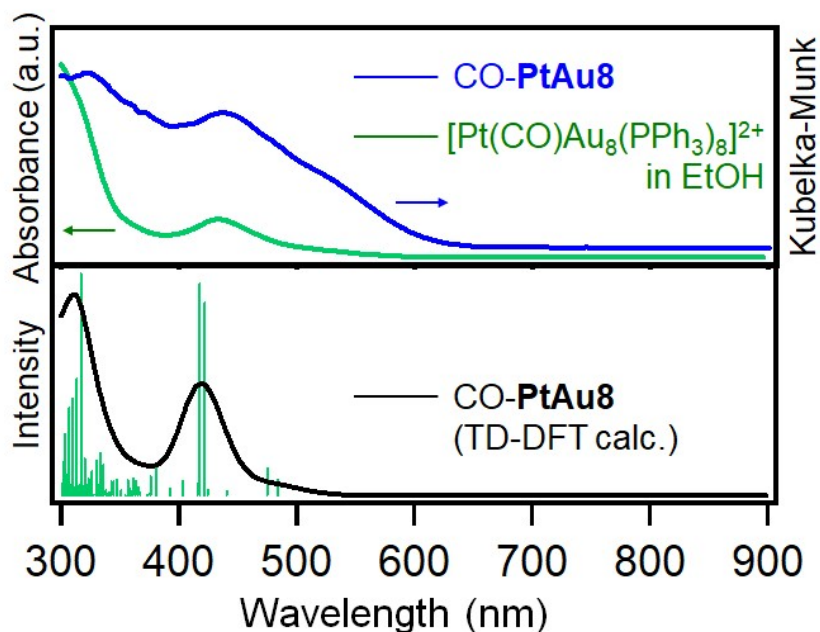


Fig. S7. UV-vis spectrum of CO adsorbed **PtAu8** ($[\text{Pt}(\text{CO})\text{Au}_8(\text{PPh}_3)_8]^{2+}$) in ethanol, DR-UV-Vis spectrum of **CO-PtAu8-PMo12**, and calculated UV-Vis spectrum using the optimized structure of **CO-PtAu8** in Fig. 3c,

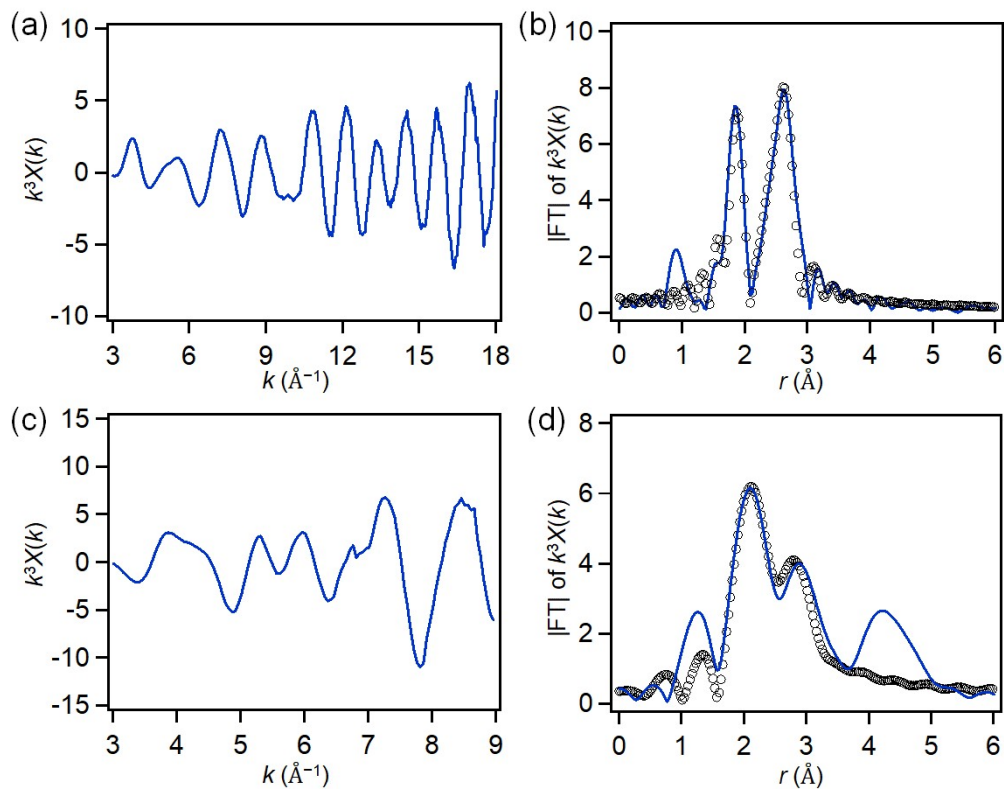


Fig. S8. Au L_3 -edge (a) EXAFS oscillation and (b) FT-EXAFS, and Pt L_3 -edge (c) EXAFS oscillation and (d) FT-EXAFS of **CO-PtAu8-PMo12** measured at 10 K. The circles in (b) and (d) represent the fitting curves, whose parameters and results are listed in Table S1.

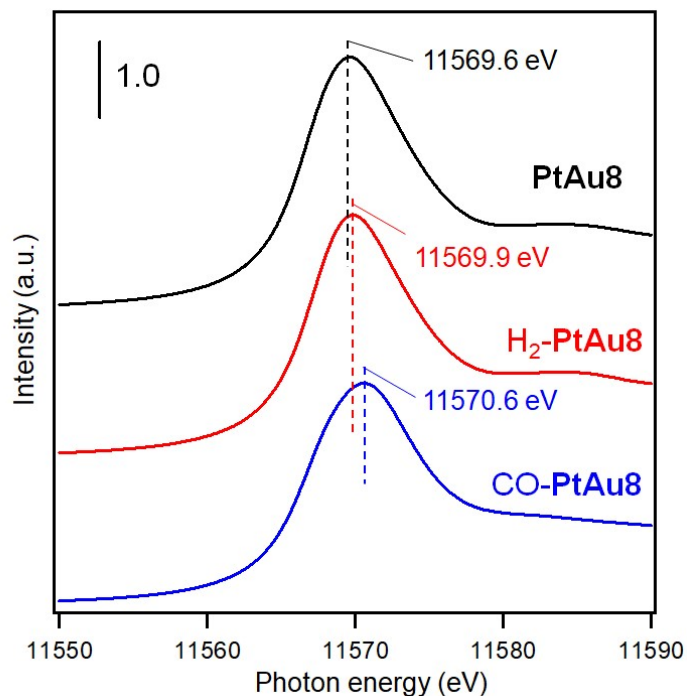


Fig. S9. Simulated Pt L_3 -edge XANES of the crown-motif **PtAu8**, **H₂-PtAu8** (using optimized structure in Fig 3f), and the chalice-motif **CO-PtAu8** (using optimized structure in Fig. 3c. Energy calibration was carried out using the peak energy (11569.6 eV) of **PtAu8-PMo12** in Fig. 3a.

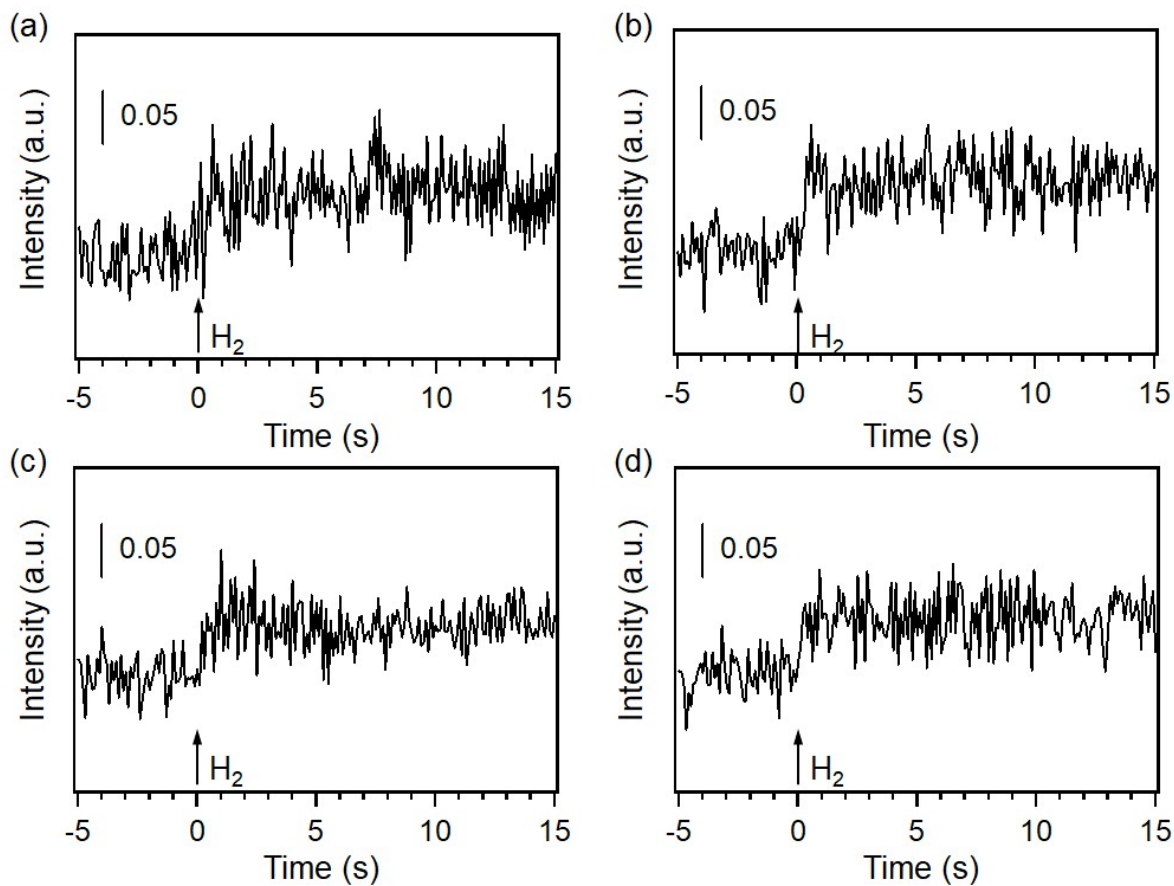


Fig. S10. Time course of peak intensity at 11570 eV in Pt L_3 -edge XANES of **PtAu8-PMo12** during H_2 introduction: (a) 1st H_2 introduction, (b) 2nd H_2 introduction after evacuation of (a), (c) 3rd H_2 introduction after evacuation of (b), (d) 4th H_2 introduction after evacuation of (c).

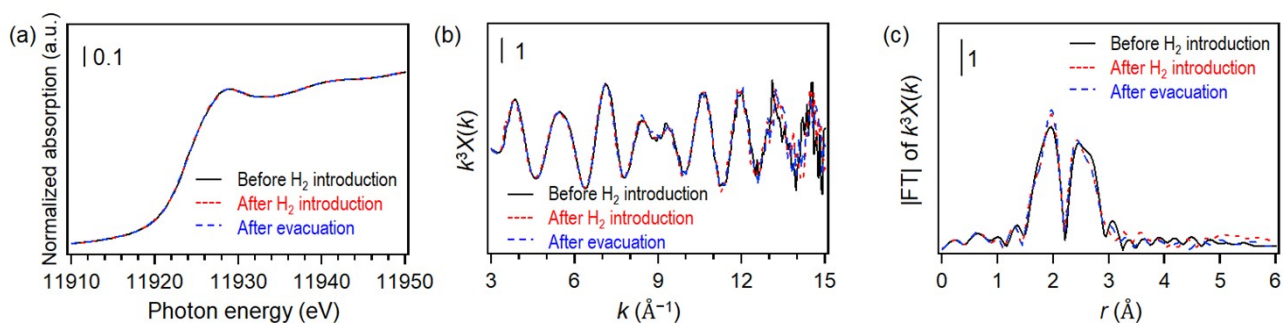


Fig. S11. Au L₃-edge (a) XANES, (b) EXAFS oscillations and (c) FT-EXAFS spectra of **Au₉-PMo₁₂** before and after H₂ introduction and after evacuation.

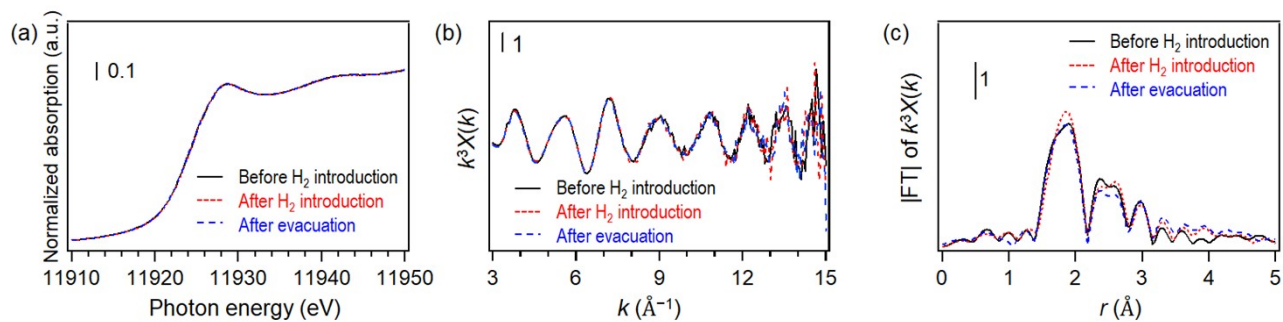


Fig. S12. Au L₃-edge (a) XANES, (b) EXAFS oscillations and (c) FT-EXAFS spectra of **PtAu₈-PMo₁₂** before and after H₂ introduction and after evacuation.

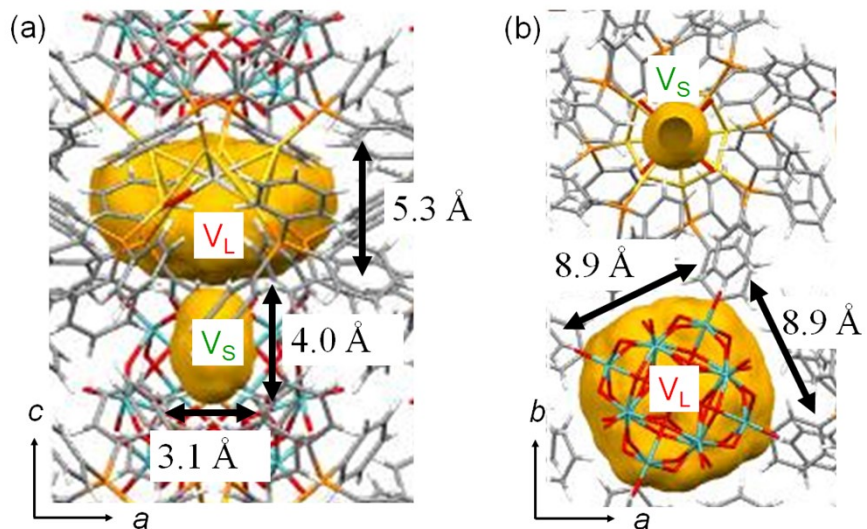


Fig. S13. Size of the closed voids in **PtAu₈-PMo₁₂**.

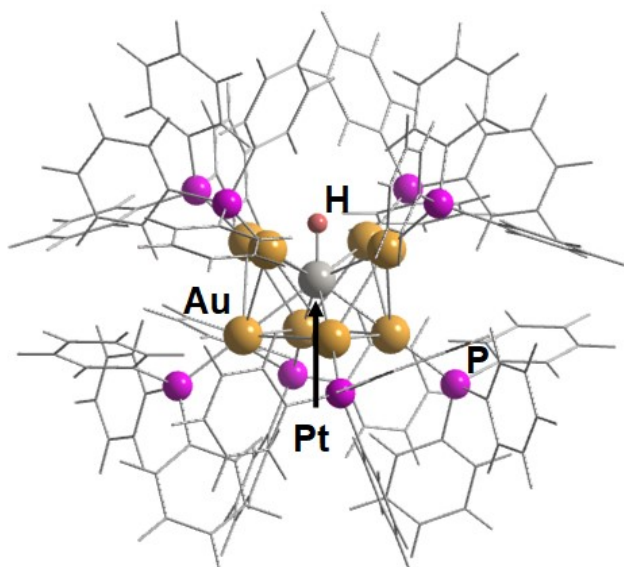


Fig. S14. Optimized structure of H-PtAu8.

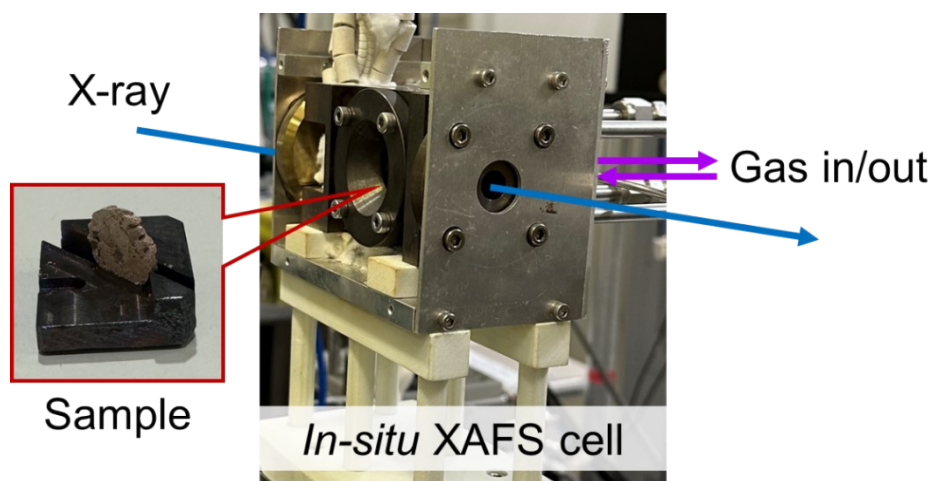
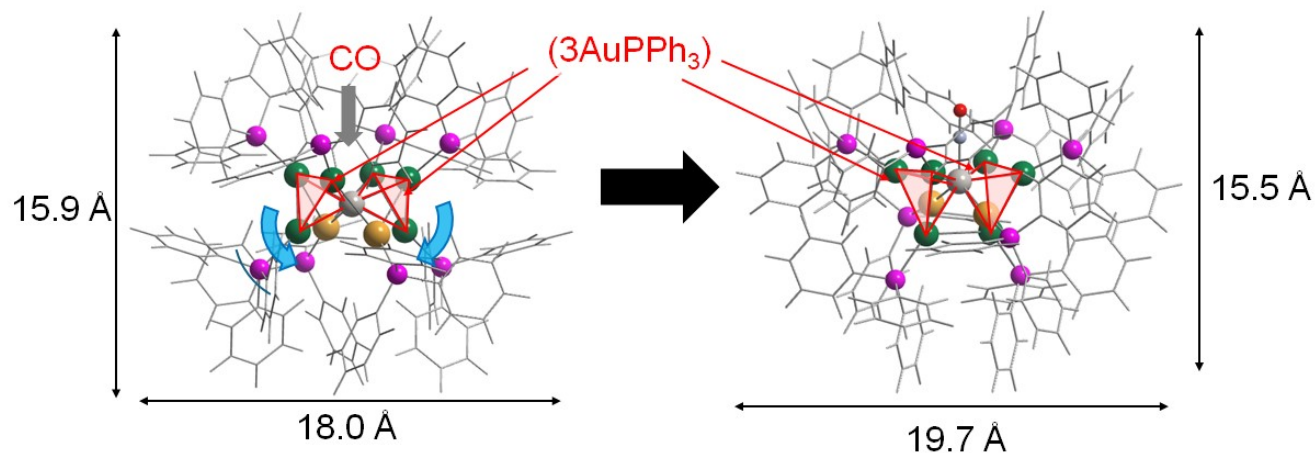


Fig. S15. Experimental setup for *in-situ* XAFS measurement of solid samples at SPring-8.



Scheme S1. Proposed structural isomerization mechanism from crown-motif PtAu8 to chalice-motif PtAu8 and cluster size obtained by optimized structures of crown-motif PtAu8 and chalice-motif PtAu8 by DFT calculations. Color; gray: Pt, green: Au in (3AuPPh₃) unit, pink: P.

Table S1. Curve fitting results of Au L₃-edge FT-EXAFS spectra for **PtAu8-PMo12**, **CO-PtAu8-PMo12**, and **Au9-PMo12**.

Samples	Bonds	CNs	r (Å)	σ^2	R-factor(%)
PtAu8-PMo12	Au-P	1.4 (2)	2.20 (3)	0.003 (2)	13.2
	Au-Pt	1.4 (1)	2.66 (2)	0.002 (1)	
	Au-Au	2.3 (2)	2.80 (2)	0.004 (2)	
CO-PtAu8-PMo12	Au-P	1.0 (2)	2.23 (3)	0.002 (1)	14.9
	Au-Pt	1.3 (1)	2.69 (2)	0.003 (1)	
	Au-Au	3.6 (7)	2.93 (11)	0.014 (11)	
Au9-PMo12	Au-P	1.4 (2)	2.28 (4)	0.004 (3)	11.4
	Au-Au1	1.4 (1)	2.67 (2)	0.003 (2)	
	Au-Au2	1.9 (2)	2.78 (3)	0.005 (2)	

CNs: coordination numbers, r : bond distance, σ^2 : Debye–Waller factor.

Numbers in parentheses represent uncertainties. The reliability factor (R-factor) is defined as:

R-factor = $\{\sum[k^3 \chi_{\text{obs}}(k) - k^3 \chi_{\text{cal}}(k)]^2 / \sum[k^3 \chi_{\text{obs}}(k)]^2\}^{1/2}$ where, χ_{obs} and χ_{cal} correspond to the observed and calculated data, respectively.

Table S2. Curve fitting results of Pt L₃-edge FT-EXAFS spectra for **PtAu8-PMo12** and **CO-PtAu8-PMo12**.

Samples	Bonds	CNs	r (Å)	σ^2	R-factor(%)
PtAu8-PMo12	Pt-Au	7.8 (3)	2.63 (3)	0.003 (2)	12.3
CO-PtAu8-PMo12	Pt-C	1.3 (3)	1.81 (10)	0.020 (17)	12.0
	Pt-Au	8.0 (4)	2.64 (3)	0.005 (4)	

CNs: coordination numbers, r : bond distance, σ^2 : Debye–Waller factor.

Numbers in parentheses represent uncertainties. The reliability factor (R-factor) is defined as:

R-factor = $\{\sum[k^3 \chi_{\text{obs}}(k) - k^3 \chi_{\text{cal}}(k)]^2 / \sum[k^3 \chi_{\text{obs}}(k)]^2\}^{1/2}$ where, χ_{obs} and χ_{cal} correspond to the observed and calculated data, respectively.

Table S3. Structural parameters of **CO-PtAu8** in Au L₃- and Pt L₃-edges obtained by the DFT calculation.

Sample	Edge	Bonds	CNs	r (Å)
[Pt(CO)Au₈(PPh₃)₈]²⁺	Au L ₃	Au-P	1.0	2.43[2.30]
		Au-Pt	1.0	2.79[2.64]
		Au-Au	3.8	3.14[2.97]
	Pt L ₃	Pt-C	1.0	1.91[1.81]
		Pt-Au	8.0	2.79[2.64]

Bond lengths determined by the average bond lengths for the model structures. Numbers in square brackets are bond lengths reduced to 94.6% of their original values.²

References

- 1 M. Schulz-Dobrick and M. Jansen, *Z. Anorg. Allg. Chem.*, 2008, **634**, 2880–2884.
- 2 Y. Fujiki, T. Matsuyama, S. Kikkawa, J. Hirayama, H. Takaya, N. Nakatani, N. Yasuda, K. Nitta, Y. Negishi and S. Yamazoe, *Commun. Chem.*, 2023, **6**, 129.